# Screening of Novel Metal Oxide Photocatalysts by Scanning Electrochemical Microscopy and Research of Their Photoelectrochemical Properties

**Wen Liu, Heechang Ye, and Allen J. Bard***

*Center for Electrochemistry, Department of Chemistry and Biochemistry, The University of Texas at Austin, Austin, Texas 78712*

*Received: October 2, 2009; Revised Manuscript Received: November 24, 2009*

Photocatalyst arrays of a number of metal oxides were prepared by dispensing metal precursor solutions onto fluorine-doped tin oxide-coated glass followed by annealing at 500 °C for 3 h. These were screened by scanning electrochemical microscopy with a scanning optical fiber, and the results showed that all Sn-doped Cd−In−Bi, Zn−In, and W−Cd oxide photocatalysts produced enhanced photocurrents for specific metal ratios. The products of the photoelectrochemical (PEC) reaction could be detected electrochemically by a Au ring on the optical fiber. The PEC properties of larger electrodes were investigated, and the Zn−In and W−Cd oxide photocatalysts showed a much higher photoactivity than Sn-doped Cd−In−Bi. Even without catalysts, they showed visible light response for water oxidation to oxygen.

## Introduction

We describe further experiments in the use of semiconductor spot arrays prepared with an automated dispenser and rapid screening by PEC-SECM (photoelectrochemical scanning electrochemical microscopy) with the discovery of several interesting metal oxide systems capable of water oxidation with visible light. Semiconductor photocatalysts have been widely investigated since Honda and Fujishima in 1972 suggested the possibility of the photoelectrochemical (PEC) splitting of water at a semiconductor electrode.[1] Since then, the search for highly efficient and stable semiconductors as photocatalysts for the splitting of water into hydrogen and oxygen using solar energy has been intensively studied. In recent years, various metal oxide, sulfide, nitride, phosphide, and selenide compounds have been reported.[2−14] The oxide photocatalysts have been especially popular, because they are stable, inexpensive, and simple to synthesize. A typical example is $TiO_2$,[15−17] with a band gap of 3.2 eV in the anatase crystalline phase, which shows relatively high photoactivity and chemical stability under ultraviolet (UV) light. However, the key problem with $TiO_2$ is its low efficiency for visible light absorption and hence most of the solar spectrum. Therefore, the search for photocatalysts with a high efficiency for application in water splitting and with good stability continues.

A PEC system provides a promising approach for converting solar energy to electricity or fuels,[18] and a larger number of PEC cells have been developed in recent years. Much work has been done with a single semiconductor PEC system, consisting, e.g., of an n-type photoanode and Pt cathode under UV irradiation; a suitable semiconductor electrode material requires stability in an electrolyte under irradiation, an appropriate band gap for the solar spectrum, and suitable band positions for water oxidation and reduction. So far, the electrode materials explored have largely been selected from transition-metal ions with a $d^0$ electronic configuration or post-transition-metal ions of $d^{10}$ configuration, along with group VA or VIA ions as counteranion components.[19−21] Different metal ions were chosen to form combined bimetallic and trimetallic (or more) compounds.

Because there are not yet predictive theoretical approaches to the selection of photocatalysts, combinatorial or rapid synthesis/screening approaches have been used.[22−25] Our group has proposed SECM as a means for the rapid synthesis and screening of electrocatalysts, such as Fe−Pd, Fe−Eu, Fe−Rb, Fe−Co, and Fe−Ni oxide photocatalysts.[26] By replacing the usual SECM ultramicroelectrode (UME) tip with an optical fiber, rapid scanning of photocatalysts, e.g., for water oxidation and hydrogen evolution, is also possible, and several good photocatalysts such as zinc-doped bismuth vanadate and tin-doped iron oxide have been found using this approach.[27,28] One end of the optical fiber was connected to a 150 W Xe lamp, and the other was placed in the SECM tip holder over the spot array at a distance of 50 $\mu$m for screening. The photocurrent detected at the spots was recorded during the scan. The different photocurrents are displayed by various colors in the SECM images, generally with yellow or brown representing higher anodic currents and green smaller ones. In this paper, several metal oxide photocatalysts were prepared and scanned using this technique.

## Experimental Section

**Materials.** FTO-coated glass was obtained from Pilkington (Toledo, OH). The 1.5 cm × 1.5 cm glass was cleaned by sonication in ethanol and rinsed with deionized water. Solutions of $InCl_3$, $Zn(NO_3)_2$, $Cd(NO_3)_2 \cdot 4H_2O$, $Bi(NO_3)_3$, $SnCl_4$ (Aldrich), and $(NH_4)_{10}W_{12}O_{41} \cdot 5H_2O$ (Strem) were used as precursors. All of these were dissolved in ethylene glycol with a metal ion concentration of 0.1 M.

**Preparation of Photocatalyst Arrays.** A CH Instruments model 1550 dispenser (Austin, TX) was used to prepare the photocatalyst arrays. The substrate (FTO) was put under the picoliter piezodispenser tip (MicroJet AB-01-60, MicroFab, Plano, TX), and the three-dimensional position was controlled by three stepping motors following a programmed pattern. The scheduled voltage pulses were applied to the dispenser to add the desired number of drops (~100 pL each) of the metal precursor solution onto the substrate. The first component was loaded and dispensed in a preprogrammed pattern. After the piezodispenser was rinsed with ethylene glycol four times, the second component was filled into the dispenser and dispensed into the existing pattern. The process was repeated when a third

10.1021/jp909470f 
Published on Web 12/22/2009

component was added. The relative number of drops of each component (~10 total) determined the spot composition. The metal oxide arrays were annealed in air at 500 °C for 3 h to form the oxides.

**Screening the Array.** The SECM setup[27] consists of a 400 $\mu$m optical fiber (FT-400-URT, 3M, St. Paul, MN) fixed in the tip holder of a CHI model 900B SECM instrument. The fiber was connected to the Xe lamp via a model 9091 five-axis fiber aligner (New Focus, San Jose, CA). The array was placed in a Teflon SECM cell with the FTO/photocatalyst working electrode exposed at the bottom through a hole sealed with an O-ring (exposed area 1.0 $cm^2$). A Pt wire counter electrode and a Ag/AgCl reference electrode were used to complete the three-electrode configuration. A 0.1 M $Na_2SO_3$/0.1 M $Na_2SO_4$ solution as a sacrificial electron donor was used as the electrolyte. The use of a sacrificial donor in the initial screening allows the observation of photocurrents that are independent of the electrocatalytic properties necessary for the more difficult water oxidation. These were then followed, for favorable materials, with 0.1 M $Na_2SO_4$ solution to study water oxidation. The optical fiber was positioned perpendicular to the working electrode surface and scanned over the surface at 500 $\mu$m/s (SECM setting 50 $\mu$m/0.1 s). A 420 nm wavelength filter was used to block the UV light in visible light illumination experiments. The optical fiber tip was held and scanned 50 $\mu$m above the working electrode surface, while a given potential was applied to the working electrode array by the SECM potentiostat. The photocurrent obtained during the scan was measured and recorded to produce a color-coded two-dimensional image.

**Au Ring Optical Fiber.** A commercial Au-coated optical fiber (Fiberguide Industries, Inc., Stirling, NJ) which was introduced[27] was used for detecting products. This was sealed in a borosilicate glass capillary by heating under vacuum. The sealing method was the same as that used in the preparation of UMEs for the usual SECM experiments.[29] The result of this procedure was an optical fiber surrounded by a Au ring electrode and a glass insulator.[30] The optical fiber core diameter ($d$), the Au ring inner $d$, the outer $d$, and the whole optical fiber including the glass insulator part $d$ were 200, 240, 275, and 600 $\mu$m, respectively. A 0.1 M $Na_2SO_4$ aqueous solution was used for testing such tips. To detect oxygen produced during the photooxidation of water at the photocatalysts arrays, the Au ring electrode was electrochemically plated with Pt by applying 0.1 V (vs Ag/AgCl) for 300 s in 1.0 mM $K_2PtCl_4$ in 0.1 M $H_2SO_4$ aqueous solution.

**Preparation and Measurement of the Photoelectrochemical Properties of a Thin Film Electrode.** Once an enhanced photocurrent was found for the PEC system in the array studies, a thin film was prepared by the spray coating method for preliminary studies of PEC properties and better characterization carried out for a film on a larger electrode. A spray gun (GP-1, Fuso Seiki Co., Ltd., Japan) was used to spray solution on a 1.5 cm × 1.5 cm FTO-coated glass on a hot plate (~300 °C). The container of the gun was filled with a premixed solution containing the metal precursors with specific compositions determined from the array results. Argon at 10 psi was used as the carrier gas. The distance between the spray nozzle and the FTO-coated glass, which was preheated to 300 °C on the hot plate, was about 20 cm. The 0.02 M mixed metal salt solution was spray coated on the FTO surface for 5 min. The thin film was then annealed at 500 °C for 3 h.

The electrochemical cell contained the thin film photoanode (0.2 $cm^2$), a Ag/AgCl reference electrode, and a Pt gauze counter electrode. The photoanode was irradiated by a Xe lamp (150 W, around 100 mW/$cm^2$). The photocurrent vs potential ($i-V$) was measured in 0.1 M $Na_2SO_3$ or 0.1 M $Na_2SO_4$ under UV or visible ($\lambda_g$ > 420 nm) irradiation. Chronoamperometry curves were obtained at 0.2 V vs Ag/AgCl for photosensitivity measurements of the electrode under dark or illuminated conditions.

**TABLE 1: Summary of Mix Effects of Different Metals Obtained by Screening the Array with SECM**

| | combination oxides |
|---|---|
| positive effect | Cd−In, Cd−Sn, Cd−Ga, Cd−W, Sn−In, Sr−In, Cu−In, Zn−In, Ga−In, Sn−Sr, Sn−Ga |
| negative effect | W−Fe, W−V, W−Zn, W−Bi, Zn−Fe, Zn−Cd, Zn−Ga, Zn−Nb, Ti−In, Fe−In, La−In, Ni−In, Fe−Ni, Fe−Ga, Bi−Mo, Bi−Zn, Bi−Ag, Bi−Ga, Bi−In, Cd−Fe, Cu−Nb |

## Results and Discussion

Our approach, as in previous studies, was to examine a wide range of compositions, with the goal of (1) finding useful new materials and (2) eventually obtaining a better understanding, through pattern recognition, of how composition affects PEC properties (e.g., band gap, band energetics). No theory currently is available that allows prediction of properties from composition. However, one must also recognize that material structure can also play a major role in observed PEC behavior. The hope is that by using a uniform method of preparation and the same substrate material (FTO) an assessment of the relative properties can be obtained.

To find good materials for water oxidation, assorted binary metal oxide combination arrays were prepared and screened. Table 1 summarizes the general effects found. Positive or negative effects on the UV−vis-light-induced photocurrent response imply a larger or smaller photocurrent, respectively, compared with those of the two pure metal oxides. From these semiquantitative studies, materials that showed the highest photocurrents were chosen for further detailed study.

**Systems Based on Cd−In−O.** Cadmium and indium are widely used in photocatalysts. Here, the photoactivity of the Cd−In−O system was optimized, and then the effect of adding additional metals was studied. In this experiment, Bi and Sn were chosen as the third and fourth components to prepare composite photocatalysts, respectively, because their oxides are known to show photocatalytic properties in previous studies.

***Cd−In−O.*** Cd−In oxide arrays were prepared with 0.1 M $Cd(NO_3)_2 \cdot 4H_2O$ as the first component and 0.1 M $InCl_3$ as the second. Arrays with metal atomic ratios from 10:0 to 0:10 (Cd:In) were screened.

Figure 1 shows the dispensed pattern of the array. The first spot in row 1 and the last spot in row 2 represent the 100% Cd

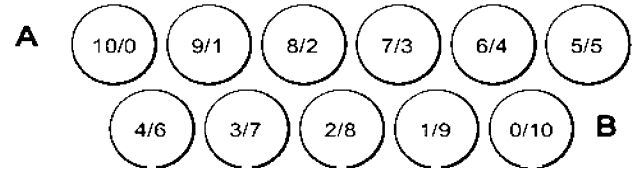


**Figure 1.** Dispensed pattern of photocatalyst arrays. The first and last spots are 100% A and 100% B. The first and second numbers inside each circle represent the number of drops of the first and second components, respectively.

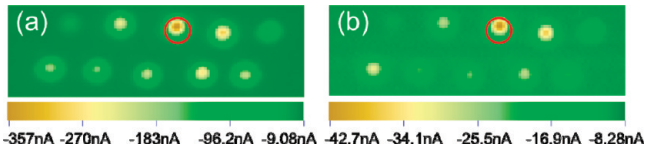


**Figure 2.** SECM images of Cd−In photocatalyst at an applied potential of 0.2 V vs Ag/AgCl in 0.1 M $Na_2SO_3$/0.1 M $Na_2SO_4$ solution under (a) UV−vis and (b) visible light illumination (>420 nm). The scan rate was 500 $\mu$m/s (SECM setting 50 $\mu$m/0.1 s), the spot size ~400 $\mu$m, and the array size 5500 $\mu$m × 1700 $\mu$m.

and 100% In. The first number in the circles is the number of drops of a solution of $Cd(NO_3)_2 \cdot 4H_2O$, and the second is the number of drops of $InCl_3$.

A given array would frequently consist of repeat patterns of these rows interspersed with rows of pure CdO and $In_2O_3$ to judge the reproducibility of the dispensing and screening results. Figure 2 shows the photocurrent obtained by screening the array by SECM in the presence of a sacrificial donor, $SO_3^{2-}$, which is easier to oxidize than water. The highest photocurrent was found with an atomic ratio of Cd:In of 7:3. Note that the photocurrent for this Cd−In oxide was 357 nA, significantly higher than those of 100% CdO (at the background level) and $In_2O_3$ (at 183 nA). Moreover, it also increased under visible light irradiation. The result indicates that the doping of In can give a positive effect to Cd. However, the photocurrent is not very high. Note that the optical fiber diameter was similar to the spot size, resulting in the center of the spots showing higher currents than the edges.

***Cd−In−Bi−O Photocatalyst.*** We also investigated trimetallic systems. For example, a higher photocurrent is obtained when $Bi(NO_3)_3$ is added to Cd−In oxide as a third component. A triangle array was used (Figure 3a). The top corner is pure CdO. The bottom left and right corners are pure $In_2O_3$ and $Bi_2O_3$, respectively. The concentrations of these were decreased by 10% compared with the adjacent column. The first, left column was composed of only Cd−In oxide, and the bottom row contained only Bi−In oxide.

Figure 3b shows a scan of the dispensed pattern of the array. Spots A, B, and C (Figure 3b) were prepared with Cd−In−Bi oxide ratios of 40:50:10, 30:60:10, and 20:70:10, respectively. They show a higher photocurrent than the other spots, about 591 nA under UV−vis light irradiation. This photocurrent is nearly 65% higher than that of the Cd−In (7:3) oxide spot in Figure 2. The spots with the ratio of Cd:In from 40:50 to 20:70 also exhibit higher activity.

***Sn-Doped Cd−In−Bi−O Photocatalyst.*** The addition of yet another metal can also increase the photoresponse. The Cd−In−Bi oxide with a ratio of 30:60:10 was selected for additional doping, because it showed one of the largest photocurrents. The ratio of this mixture was fixed to prepare arrays as the first component, and $SnCl_4$ was chosen as the second component.

Figure 4 shows that addition of Sn leads to a much higher photocurrent. With an increase of Sn, the photocurrent of the mixture increased first and then decreased. When the ratio of Cd−In−Bi oxide versus Sn was equal to 60:40, i.e., for Sn:Cd:In:Bi = 40:18:36:6, the highest photocurrent, 1150 nA under UV−vis light irradiation and 117 nA under visible (>420 nm) light irradiation, respectively, was found. This photocurrent is 222% higher than that of Cd−In oxide and 95% higher than that of Cd−In−Bi oxide under UV−vis light irradiation. Even under visible light, it also increased and was about 174% higher than that of Cd−In oxide (Sn-doped Cd−In−Bi oxide, 117 nA, versus Cd−In oxide, 42.7 nA).

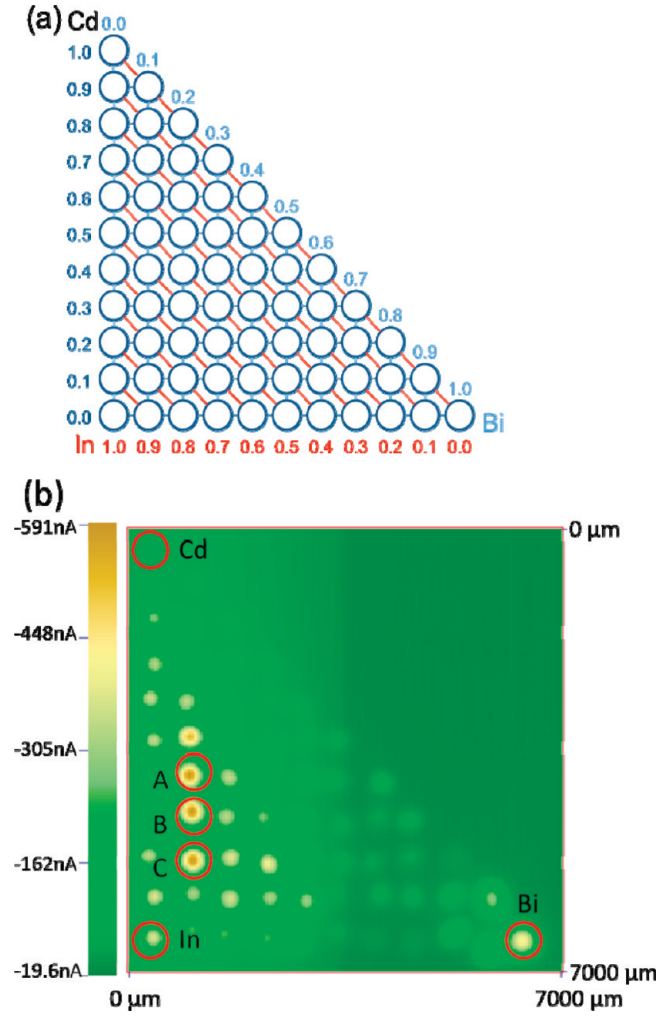


**Figure 3.** Dispensed pattern of photocatalyst arrays (a) and SECM images of Cd−In−Bi photocatalyst (b) at 0.2 V vs Ag/AgCl applied potential in 0.1 M $Na_2SO_3$/0.1 M $Na_2SO_4$ solution under UV−vis light illumination. In the array, the top corner is 100% Cd, the bottom left corner is 100% In, and the bottom right corner is 100% Bi. Spots A, B, and C represent Cd−In−Bi of 40:50:10, 30:60:10, and 20:70:10 (atom %) ratios, respectively. The scan rate was 500 $\mu$m/s (SECM setting 50 $\mu$m/0.1 s) and the spot size ~400 $\mu$m.

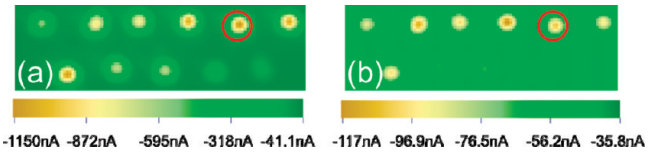


**Figure 4.** SECM images of Sn-doped Cd−In−Bi photocatalyst at an applied potential of 0.2 V vs Ag/AgCl in 0.1 M $Na_2SO_3$/0.1 M $Na_2SO_4$ solution under (a) UV−vis and (b) visible light illumination. The scan rate was 500 $\mu$m/s (SECM setting 50 $\mu$m/0.1 s), the spot size ~400 $\mu$m, and the array size 5500 $\mu$m × 1700 $\mu$m.

**Zn−In−O Photocatalyst.** ZnO has been investigated extensively and is capable of producing a good photoresponse in the UV region. In this study, In was added to Zn to enhance the performance of its photoactivity. Here, $InCl_3$ as component 2 was added to $Zn(NO_3)_2$ to prepare a sample of In-doped ZnO and screened. Figure 5, with the same layout as Figure 1 with pure ZnO on the upper left and $In_2O_3$ on the lower right, indicates the results of the screening. The photocurrents of pure ZnO (the first spot in row 1) under UV−vis and visible light irradiation, respectively, are 295 nA and background current (because of its wide band gap). These are lower than the

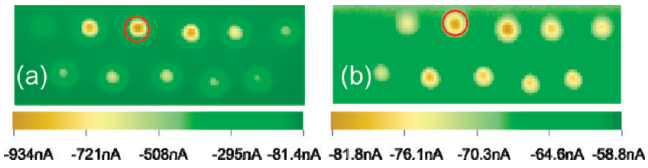


**Figure 5.** SECM images of Zn−In photocatalyst at an applied potential of 0.2 V vs Ag/AgCl in 0.1 M $Na_2SO_3$/0.1 M $Na_2SO_4$ solution under (a) UV−vis and (b) visible light illumination. The scan rate was 500 $\mu$m/s (SECM setting 50 $\mu$m/0.1 s), the spot size ~400 $\mu$m, and the array size 5500 $\mu$m × 1700 $\mu$m.

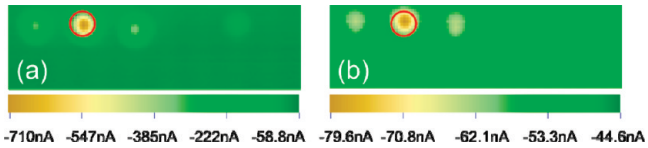


**Figure 6.** SECM images of W−Cd photocatalyst at an applied potential of 0.2 V vs Ag/AgCl in 0.1 M $Na_2SO_3$/0.1 M $Na_2SO_4$ solution under (a) UV−vis and (b) visible light illumination. The scan rate was 500 $\mu$m/s (SECM setting 50 $\mu$m/0.1 s), the spot size ~400 $\mu$m, and the array size 5500 $\mu$m × 1700 $\mu$m.

photocurrents of pure $In_2O_3$ (the last spot in row 2), which are 508 and 70.3 nA, respectively. The highest photoresponse spot composed of Zn and In with the atom ratio 80:20 gives photocurrents of 934 nA under UV−vis light (Figure 5a) and 81.8 nA under visible light (Figure 5b) irradiation. Therefore, the photocurrent increased by 217% compared to that of pure ZnO and 84% compared to that of pure $In_2O_3$ under UV−vis light irradiation. Under visible light irradiation, it was much larger than that of pure ZnO (81.8 nA versus background photocurrent) and was 16.4% higher than that of pure $In_2O_3$.

**W−Cd−O Photocatalyst.** $WO_3$ is also a well-known stable photocatalyst that can be easily produced and modified and is a good candidate for doping with other metals. A $WO_3$ array was prepared with $(NH_4)_{10}W_{12}O_{41}\cdot 5H_2O$ as the first component and $Cd(NO_3)_2\cdot 4H_2O$ as the second. The first spot in row 1 of Figure 6 is pure $WO_3$, while the last spot in row 2 is pure CdO. The photocurrents of pure $WO_3$ are 385 nA under UV−vis light irradiation and 62.1 nA under visible light irradiation, while pure CdO shows a background photocurrent. The highest photocurrent appeared when the atom ratio of W and Cd was 90:10, which is 710 nA under UV−vis light and 79.6 nA under visible light irradiation, 85% and 28% higher than those of the pure W or In oxides, respectively.

**Detection of Products.** The experiments described earlier were carried out in the presence of a sacrificial electron donor, $SO_3^{2-}$, but it is also possible to study their behavior for water photooxidation in a 0.1 M $Na_2SO_4$ aqueous solution (pH ≈ 6). A platinized Au ring electrode around the optical fiber as described in the Experimental Section, held at −0.2 V vs Ag/AgCl, was used to detect the product generated in the photoelectrochemical experiment, $O_2$. In the photooxidation of water on the surface of photocatalyst spots in 0.1 M $Na_2SO_4$ solution, the product ($O_2$) was electrochemically detected on the tip by the $O_2$ reduction reaction (ORR). In this process, the Pt ring electrode was used because of its good electrocatalytic properties for the ORR. The SECM images on the Sn-doped Cd−In−Bi oxide, Zn−In oxide, and W−Cd oxide arrays in 0.1 M $Na_2SO_4$ aqueous solutions were obtained. Figures 7−9 show the SECM images of both the substrate photocurrent (a) and the tip current (b). The applied potentials were 0.4 and −0.2 V versus Ag/AgCl for the substrate and the tip, respectively. Here, $OH^-$ is oxidized to $O_2$ on the substrate under illumination, and the generated $O_2$ is reduced on the Pt ring electrode. As a result,

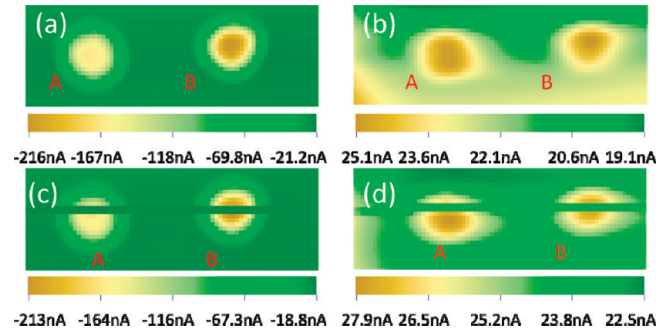


**Figure 7.** SECM images of Sn-doped Cd−In−Bi oxide photocatalysts on the substrate at 0.4 V vs Ag/AgCl (a, c) and on the tip at −0.2 V vs Ag/AgCl (b, d) under UV−vis light illumination in 0.1 M $Na_2SO_4$ solution. The light was blocked during the middle of the scan (c, d). Spots A and B contain metal ions with Sn:Cd:In:Bi ratios of 35:19.5:39:6.5 and 40:18:36:6, respectively. The scan rate was 100 $\mu$m/s (SECM setting 30 $\mu$m/0.3 s), the spot size ~400 $\mu$m, and the array size 2000 $\mu$m × 800 $\mu$m.

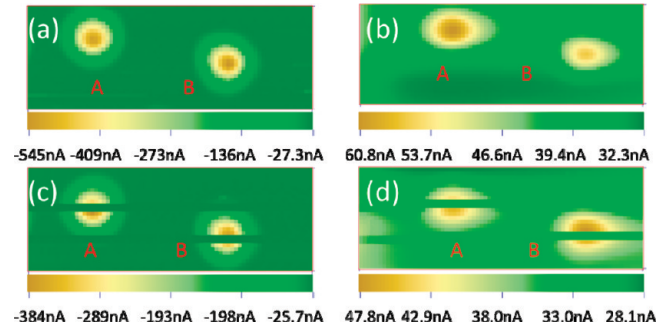


**Figure 8.** SECM images of Zn−In oxide photocatalysts on the substrate at 0.4 V vs Ag/AgCl (a, c) and on the tip at −0.2 V vs Ag/AgCl (b, d) under UV−vis light illumination in 0.1 M $Na_2SO_4$ solution. The light was blocked during the middle of the scan (c, d). Spots A and B contain Zn and In with ratios of 80:20 and 75:25, respectively. The scan rate was 100 $\mu$m/s (SECM setting 30 $\mu$m/0.3 s), the spot size ~400 $\mu$m, and the array size 2000 $\mu$m × 800 $\mu$m.

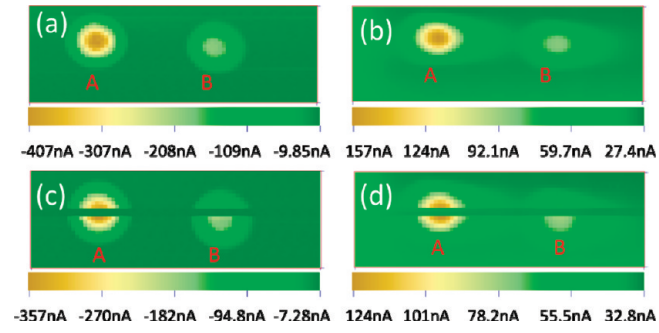


**Figure 9.** SECM images of W−Cd oxide photocatalysts on the substrate at 0.4 V vs Ag/AgCl (a, c) and on the tip at −0.2 V vs Ag/AgCl (b, d) under UV−vis light illumination in 0.1 M $Na_2SO_4$ solution. The light was blocked during the middle of the scan (c, d). Spots A and B contain W and Cd with ratios of 95:5 and 90:10, respectively. The scan rate was 100 $\mu$m/s (SECM setting 30 $\mu$m/0.3 s), the spot size ~400 $\mu$m, and the array size 2000 $\mu$m × 800 $\mu$m.

two separate images were obtained as (a) and (b) of Figures 7−9. In (c) and (d) of these figures, the same scan was carried out with the illuminated light blocked in the middle of the scanning process. This cut the photocurrent from the spots and the reduction current at the tips. This result confirms that the current with the round spot shape in the SECM images is indeed generated by the light. The drop in current at the tip was synchronous with the drop in photocurrent, as expected. The ability to observe products of the photoreaction should allow

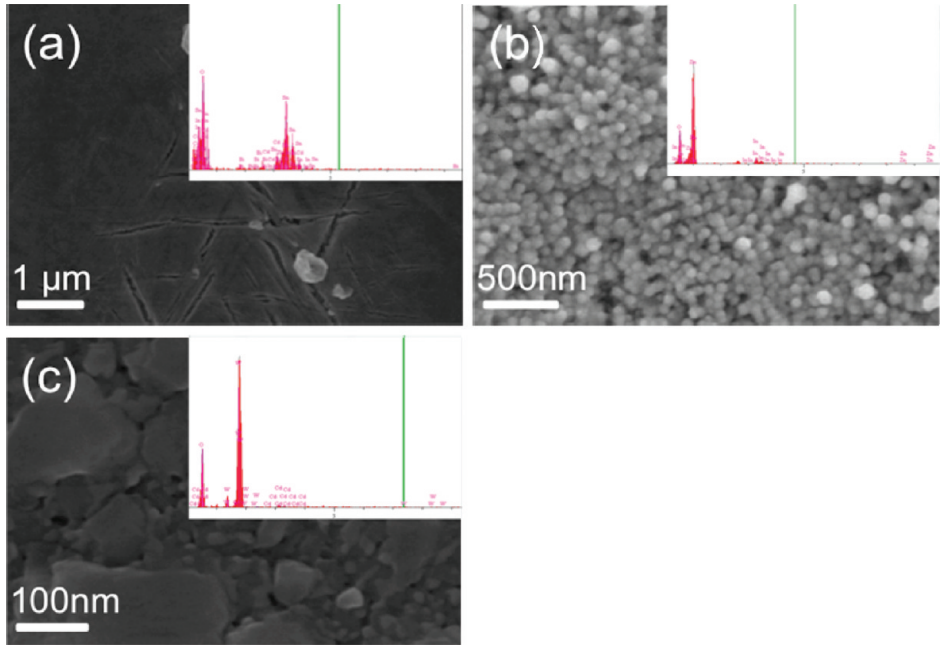


**Figure 10.** SEM images of Sn-doped Cd−In−Bi (a), Zn−In (b), and W−Cd (c) oxide photocatalysts prepared with the spray coating method.

quantitative measurements in this substrate generation/tip collection mode, which is a function of the size of the spot and the detecting tip. Simulations and applications of this mode are envisioned.

**Photoelectrochemical Properties of a Thin Film Electrode.** Because the rapid synthesis and screening process can only give an indication of the approximate compositions that might produce favorable photocurrents, upon discovery of interesting materials, it is necessary to make a larger electrode using a more careful synthesis method, as well as to characterize the material and test it in a larger PEC cell. In other words, it is necessary to confirm the SECM results with those of thin films or bulk materials of the same composition prepared with different methods on a larger electrode. First experiments like these were carried out with metal ion ratios of the photocatalysts of Sn:Cd:In:Bi = 40:18:36:6, Zn:In = 80:20, and W:Cd = 90:10.

***Characterization.*** Figure 10 shows the morphology (obtained by SEM) of a thin film electrode prepared by spray coating, which was described in the Experimental Section. The surface of the Sn-doped Cd−In−Bi (Figure 10a) oxide photocatalyst had some cracks. The Zn−In (Figure 10b) oxide photocatalyst formed nanoparticles with a diameter from 50 to 100 nm on FTO-doped glass, while the W−Cd (Figure 10c) oxide photocatalyst formed flakes. Clearly the surface area of the Zn−In and W−Cd oxide photocatalysts prepared by spray coating is larger than that of the Sn-doped Cd−In−Bi oxide photocatalyst.

Energy-dispersive X-ray spectroscopy (EDS) analysis showed the elemental compositions used for preparing thin film samples were essentially the same as the compositions of the mixed solutions used. Alternative methods of preparation and more detailed characterization of these materials are planned.

***Investigation of Photoelectrochemical Properties of Photocatalysts.*** To detect the photoelectrochemical properties, the prepared thin film electrodes were positioned in a Teflon cell to facilitate the transmittance of light to the photoelectrode surface and were irradiated with a Xe lamp (150 W) at the same time. The active surface area of the working electrode, which was defined by a rubber O-ring, was 0.2 $cm^2$. A platinum gauze and a Ag/AgCl electrode were used as counter and reference electrodes, respectively.

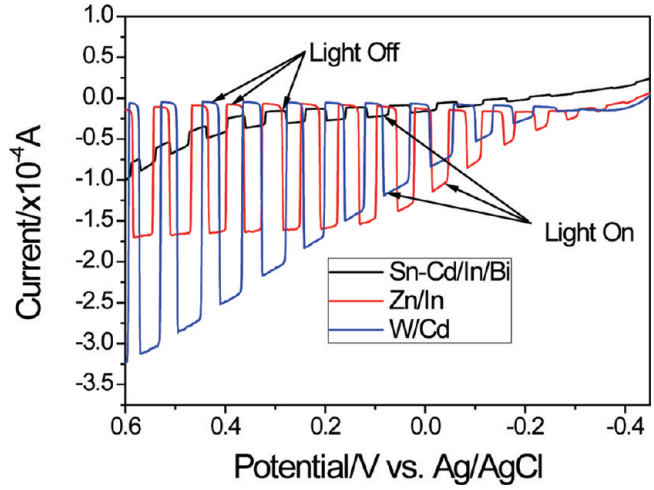


**Figure 11.** Chopped photocurrent−potential curves of Sn-doped Cd−In−Bi (dark), Zn−In (red), and W−Cd (blue) oxide photocatalyst thin film electrodes under UV−vis light irradiation (sacrificial donor, 0.1 M $Na_2SO_3$; light source, 150 W Xe lamp; sweep rate, 20 mV/s).

At first, the 0.1 M $Na_2SO_3$ solution was chosen as a sacrificial electron donor for measurement, because it was necessary to make sure the results obtained from the thin film photoelectrochemical test and the array screening experiment were coincident. The thin film electrodes with different oxide photocatalysts showed different photocurrents over a potential range of −0.30 to +0.60 V, as shown in Figure 11. The onset photopotential was about −0.30 V vs Ag/AgCl. The Sn-doped Cd−In−Bi oxide photocatalyst showed a much lower photocurrent than the other two electrodes, 125 $\mu A/cm^2$ at 0.2 V vs Ag/AgCl in 0.1 M $Na_2SO_3$ solution under UV−vis light irradiation compared to 850 $\mu A/cm^2$ and 900 $\mu A/cm^2$ for Zn−In or W−Cd oxide photocatalysts, respectively. The W−Cd thin film electrode was the best photocatalyst among the three under UV−vis light irradiation.

Figure 12 compares the current−time transient responses of Sn-doped Cd−In−Bi, Zn−In, and W−Cd oxide photocatalyst thin film electrodes under visible ($\lambda_g$ > 420 nm) and UV−vis illumination conditions. All of them showed good photosensitiv-

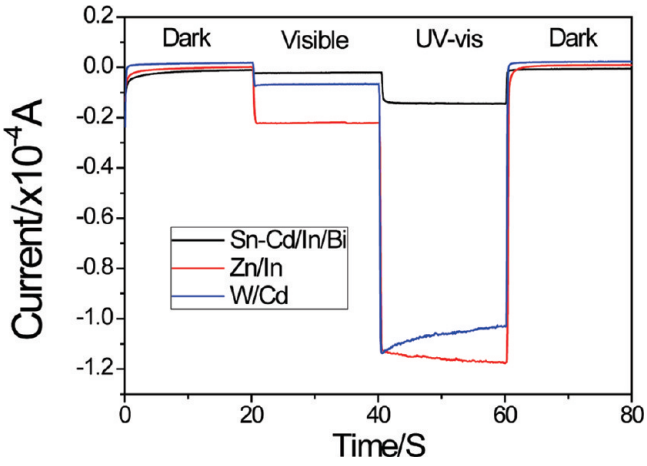


**Figure 12.** Current−time transient response of Sn-doped Cd−In−Bi (black), Zn−In (red), and W−Cd (blue) oxide photocatalyst thin film electrodes under dark (0−20 and 60−80 s), visible (20−40 s), and UV−vis (40−60 s) light irradiation (sacrificial donor, 0.1 M $Na_2SO_3$; light source, 150 W Xe lamp; applied potential, 0.2 V vs Ag/AgCl).

ity and stability under UV−vis and visible light. The highest photocurrent occurred under UV−vis light irradiation, followed by the current under visible light irradiation, while the dark current was negligible in 0.1 M $Na_2SO_3$ solution. The Sn-doped Cd−In−Bi oxide photocatalyst showed a low photocurrent under UV−vis light and negligibly small photocurrent under visible light ($\lambda_g$ > 420 nm) compared with the other two photocatalysts, so the Zn−In and W−Cd oxides were chosen for further study. In addition, the relative photocurrents under visible light irradiation of Zn−In and W−Cd oxide photocatalysts were 20% and 10%, respectively, compared with those under UV−vis light irradiation.

Preliminary experiments were also carried out with 0.1 M $Na_2SO_4$ as the electrolyte solution. Because our final goal is water splitting with prepared oxide photocatalysts, it is necessary to investigate the photoactivity of them in $Na_2SO_4$ solution. In this case, $OH^-$ was oxidized to generate $O_2$ at a pH of ~6. The other conditions of this measurement were the same as the earlier ones with $SO_3^{2-}$. Figure 13 shows that the onset photopotential of Zn−In oxide photocatalyst was −0.20 V vs Ag/AgCl (Figure 13a) while it was 0.05 V vs Ag/AgCl for W−Cd oxide photocatalyst (Figure 13b). The photocurrents of Zn−In and W−Cd oxide photocatalysts were 90 and 100 $\mu$A/cm$^2$ under UV−vis light irradiation, respectively, at 0.2 V vs Ag/AgCl (compared to the thermodynamic onset of $O_2$ evolution at this pH of 0.7 V vs Ag/AgCl) in 0.1 M $Na_2SO_4$ solution. While under visible light irradiation, the photocurrents were 20 and 10 $\mu$A/cm$^2$, respectively. Thus, the visible light response of Zn−In oxide photocatalyst is better than that of W−Cd oxide photocatalyst, while it is worse under UV−vis light irradiation, which is consistent with previous results.

Figure 14 shows the current−time transient responses of the two photocatalysts under visible ($\lambda_g$ > 420 nm) and UV−vis light irradiation in 0.1 M $Na_2SO_4$ solution at 0.2 V vs Ag/AgCl. For water oxidation, the photocurrents of Zn−In and W−Cd oxide photocatalysts were 20% and 10% under visible light irradiation compared to those under UV−vis light irradiation, respectively. Note that the smaller apparent fill factors seen for water oxidation are probably the result of slower heterogeneous kinetics compared to that of $SO_3^{2-}$, so experiments with a water oxidation catalyst on the semiconductor surface are being planned.

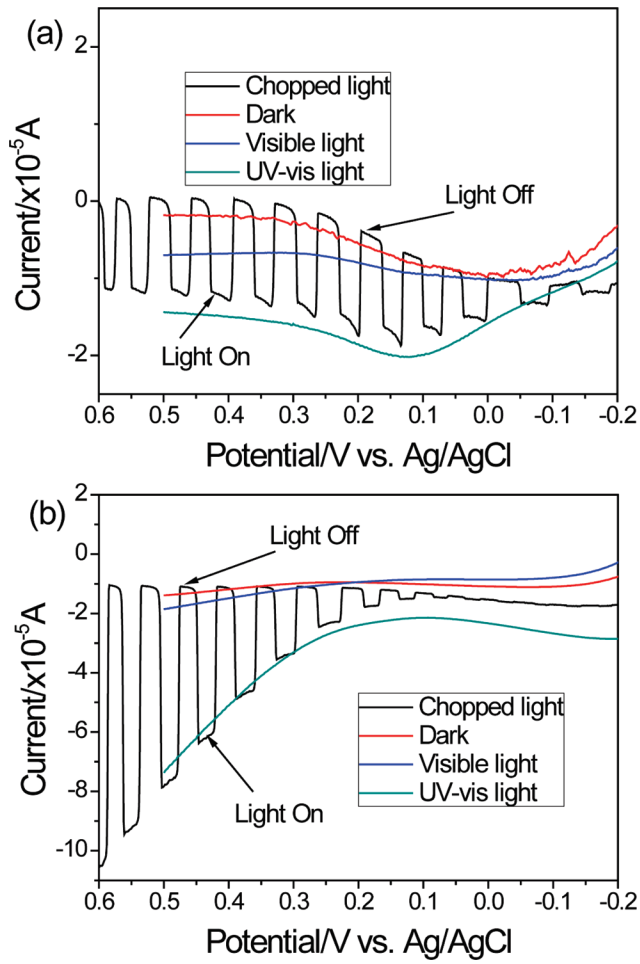


**Figure 13.** Photocurrent−potential curves of Zn−In (a) and W−Cd (b) oxide photocatalyst thin film electrodes under chopped, dark, visible, and UV−vis light irradiation (electrolyte solution, 0.1 M $Na_2SO_4$; light source, 150 W Xe lamp).

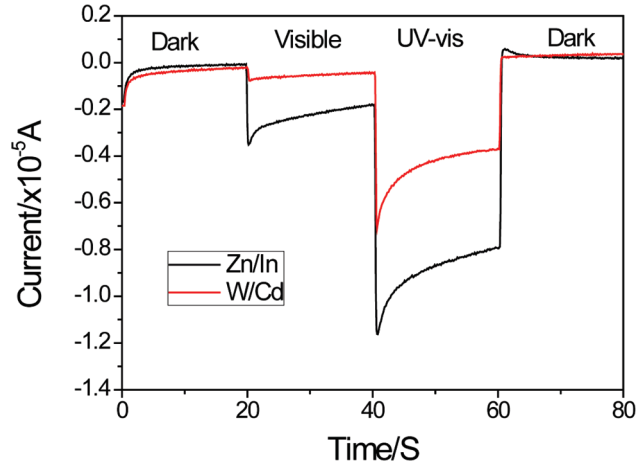


**Figure 14.** Current−time transient response of Zn−In (black) and W−Cd (red) oxide photocatalyst thin film electrodes under dark (0−20 and 60−80 s), visible (20−40 s), and UV−vis (40−60 s) light irradiation (electrolyte solution, 0.1 M $Na_2SO_4$; light source, 150 W Xe lamp; applied potential, 0.2 V vs Ag/AgCl).

## Conclusions

Photocatalyst arrays were prepared by dispensing different amounts of metal precursor solutions onto FTO-coated glass with a CH Instruments model 1550 dispenser. Then they were screened by SECM, and the results showed that the Sn-doped

Cd−In−Bi, Zn−In, and W−Cd oxide photocatalysts gave the highest photocurrent when the metal ratios were 40:18:36:6, 80:20, and 90:10, respectively. These were tested for photooxidation of sulfite and water. Furthermore, the product of the photoelectrochemical reaction for water oxidation, $O_2$, was detected by a Au ring optical fiber.

Their photoelectrochemical properties were investigated, and the Zn−In (80:20) and W−Cd (90:10) oxide photocatalysts showed much higher photoactivity than Sn-doped Cd−In−Bi (40:18:36:6). For water oxidation, the visible light responses of Zn−In and W−Cd are 20% and 10%, respectively, of the full UV−vis.

**Acknowledgment.** We appreciate the support of this research by the National Science Foundation (Grant CHE-0934450) and the Robert A. Welch Foundation (Grants F-0021 and H−F-0037). W.L. thanks the National Scholarship Fund of the China Scholarship Council for support and advisor Prof. Fengbao Zhang from Tianjin University. Helpful discussions with Fu-Ren F. Fan are also gratefully acknowledged.

## References and Notes

(1) Fujishima, A.; Honda, K. *Nature* **1972**, *238*, 37.
(2) Park, J. H.; Kim, S.; Bard, A. J. *Nano Lett.* **2006**, *6*, 24.
(3) Irie, H.; Watanabe, Y.; Hashimoto, K. *J. Phys. Chem. B* **2003**, *107*, 5483.
(4) Asahi, R.; Morikawa, T.; Ohwaki, T.; Aoki, K.; Taga, Y. *Science* **2001**, *293*, 269.
(5) Koji, S.; Masahiro, T.; Takashi, K.; Toshiki, A.; Masayuki, Y. *J. Phys. Chem. C* **2007**, *111*, 11636.
(6) Haram, S.; Bard, A. J. *J. Phys. Chem. B* **2001**, *105*, 8192.
(7) Zong, X.; Yan, H.; Wu, G.; Ma, G.; Wen, F.; Wang, L.; Li, C. *J. Am. Chem. Soc.* **2008**, *130*, 7176.
(8) Groenewolt, M.; Antonietti, M. *Adv. Mater.* **2005**, *17*, 1789.
(9) Maeda, K.; Domen, K. *J. Phys. Chem. C* **2007**, *111*, 7851.
(10) Ishikawa, A.; Takata, T.; Matsumura, T.; Kondo, J. N.; Hara, M.; Kobayashi, H.; Domen, K. *J. Phys. Chem. B* **2004**, *108*, 2637.
(11) Asahi, R.; Morikawa, T.; Ohwaki, T.; Aoki, K.; Taga, Y. *Science* **2001**, *293*, 269.
(12) Sartoretii, C. J.; Alexander, B. D.; Solarska, R.; Rutkowska, I. A.; Augustynski, J.; Cerny, R. *J. Phys. Chem. B* **2005**, *109*, 13685.
(13) Larson, W. L.; Maruska, H. P.; Stevenson, D. A. *J. Electrochem. Soc.* **1974**, *121*, 1673.
(14) Pan, A.; Liu, R.; Sun, M.; Ning, C.-Z. *J. Am. Chem. Soc.* **2009**, *131*, 9502.
(15) Hadjiivanov, K. I.; Klissurski, D. K. *Chem. Soc. Rev.* **1996**, *25*, 61.
(16) Heller, A. *Acc. Chem. Res.* **1995**, *28*, 503.
(17) Linsebigler, A.; Lu, G.; Yates, J. T. *Chem. Rev.* **1995**, *95*, 735.
(18) Bard, A. J.; Whitesides, G. M.; Zare, R. N.; McLafferty, F. W. *Acc. Chem. Res.* **1995**, *28*, 91.
(19) Kim, Y. I.; Salim, S.; Huq, M. J.; Mallouk, T. E. *J. Am. Chem. Soc.* **1991**, *113*, 9561.
(20) Tsuji, I.; Kato, H.; Kobayashi, H.; Kudo, A. *J. Am. Chem. Soc.* **2004**, *126*, 13406.
(21) Tsuji, I.; Kato, H.; Kudo, A. *Angew. Chem., Int. Ed.* **2005**, *44*, 3565.
(22) Woodhouse, M.; Herman, G. S.; Parkinson, B. A. *Chem. Mater.* **2005**, *17*, 4318.
(23) Woodhouse, M.; Parkinson, B. A. *Chem. Mater.* **2008**, *20*, 2495.
(24) Baeck, S. H.; Jaramillo, T. F.; Brändli, C.; McFarland, E. W. *J. Comb. Chem.* **2002**, *4*, 563.
(25) Jaramillo, T. F.; Baeck, S. H.; Kleiman-Schwarsctein, A.; Choi, K. S.; Stucky, G. D.; McFarland, E. W. *J. Comb. Chem.* **2005**, *7*, 264.
(26) Fernandez, J. L.; Walsh, D. A.; Bard, A. J. *J. Am. Chem. Soc.* **2005**, *127*, 357.
(27) Lee, J.; Ye, H.; Pan, S.; Bard, A. *J. Anal. Chem.* **2008**, *80*, 7445.
(28) Jang, J. S.; Lee, J.; Ye, H.; Fan, F. F.; Bard, A. J. *J. Phys. Chem. C* **2009**, *113*, 6719.
(29) Bard, A. J.; Mirkin, M. V. *Scanning Electrochemical Microscopy*; Marcel Dekker: New York, 2001.
(30) Lee, Y.; Bard, A. *J. Anal. Chem.* **2002**, *74*, 3626.

JP909470F